

Estimation and mapping of above-ground biomass of mangrove forests and their replacement land uses in the Philippines using Sentinel imagery



Jose Alan A. Castillo ^{a,b,d,*}, Armando A. Apan ^{a,b}, Tek N. Maraseni ^b, Severino G. Salmo III ^c

^a School of Civil Engineering and Surveying, University of Southern Queensland (USQ), QLD 4350, Australia

^b Institute for Agriculture and the Environment, USQ, QLD 4350, Australia

^c Department of Environmental Science, Ateneo de Manila University, Quezon City 1101, Philippines

^d Mangrove and Beach Forest Research Section, Ecosystems Research and Development Bureau, Los Baños 4031, Philippines

ARTICLE INFO

Article history:

Received 27 March 2017

Received in revised form 25 October 2017

Accepted 27 October 2017

Keywords:

Sentinel imagery
Biomass
Mangrove
Philippines
Biomass mapping
Land use change

ABSTRACT

The recent launch of the Sentinel-1 (SAR) and Sentinel-2 (multispectral) missions offers a new opportunity for land-based biomass mapping and monitoring especially in the tropics where deforestation is highest. Yet, unlike in agriculture and inland land uses, the use of Sentinel imagery has not been evaluated for biomass retrieval in mangrove forest and the non-forest land uses that replaced mangroves. In this study, we evaluated the ability of Sentinel imagery for the retrieval and predictive mapping of above-ground biomass of mangroves and their replacement land uses. We used Sentinel SAR and multispectral imagery to develop biomass prediction models through the conventional linear regression and novel Machine Learning algorithms. We developed models each from SAR raw polarisation backscatter data, multispectral bands, vegetation indices, and canopy biophysical variables. The results show that the model based on biophysical variable Leaf Area Index (LAI) derived from Sentinel-2 was more accurate in predicting the overall above-ground biomass. In contrast, the model which utilised optical bands had the lowest accuracy. However, the SAR-based model was more accurate in predicting the biomass in the usually deficient to low vegetation cover non-forest replacement land uses such as abandoned aquaculture pond, cleared mangrove and abandoned salt pond. These models had 0.82–0.83 correlation/agreement of observed and predicted value, and root mean square error of 27.8–28.5 Mg ha⁻¹. Among the Sentinel-2 multispectral bands, the red and red edge bands (bands 4, 5 and 7), combined with elevation data, were the best variable set combination for biomass prediction. The red edge-based Inverted Red-Edge Chlorophyll Index had the highest prediction accuracy among the vegetation indices. Overall, Sentinel-1 SAR and Sentinel-2 multispectral imagery can provide satisfactory results in the retrieval and predictive mapping of the above-ground biomass of mangroves and the replacement non-forest land uses, especially with the inclusion of elevation data. The study demonstrates encouraging results in biomass mapping of mangroves and other coastal land uses in the tropics using the freely accessible and relatively high-resolution Sentinel imagery.

© 2017 International Society for Photogrammetry and Remote Sensing, Inc. (ISPRS). Published by Elsevier B.V. All rights reserved.

1. Introduction

Mangroves are an important coastal resource in the tropics. They provide many ecosystem goods and services including the provision of wood for construction and fuel, habitat of coastal fauna and nursery of juvenile marine organisms, carbon (C) storage

in biomass and soil, protection from strong winds during typhoons and coastal erosion mitigation (Alongi, 2009; Donato et al., 2011). However, there has been a large reduction in the global mangrove forest cover due to conversion to non-forest land uses such as aquaculture, perennial agriculture and clearing for human settlement (FAO, 2007). This is especially true in tropical Southeast Asia where more than 100,000 ha of mangroves were deforested and converted to other land uses during the last 15 years, notably for aquaculture and agriculture (Richards and Friess, 2016). It is

* Corresponding author at: School of Civil Engineering and Surveying, University of Southern Queensland (USQ), QLD 4350, Australia.

E-mail addresses: Alan.Castillo@usq.edu.au, allan536@yahoo.com (J.A.A. Castillo).

crucial, therefore, to monitor the mangroves against land use change and forest degradation.

Empirical studies that quantify the carbon stocks of mangroves and the land uses that replaced them are needed in order to provide emission estimates based on actual measures of carbon stocks and reduce the uncertainty of the estimate. In addition, climate mitigation programs such as Reducing Emissions from Deforestation and Forest Degradation Plus (REDD+) are being proposed to prevent large emissions from deforestation and forest degradation in the tropics. These programs will require accurate assessment and mapping to establish the baseline biomass and C stocks against which to monitor future changes (Maraseni et al., 2005). Integrated coastal management would also require relevant maps such as biomass maps for better planning and decision-making.

Above-ground biomass is one of the important carbon pools in mangrove ecosystem (Kauffman and Donato, 2012; Howard et al., 2014). There has been a growing body of literature on mangrove biomass and their carbon stocks (e.g. Donato et al., 2011; Abino et al., 2014; Tue et al., 2014; Phang et al., 2015; Stringer et al., 2015; Vien et al., 2016). However, only a few studies have quantified biomass and carbon stock of mangrove forest side by side their replacement land uses such as aquaculture pond (Kauffman et al., 2013; Bhomia et al., 2016; Duncan et al., 2016) and cattle pastures (Kauffman et al., 2016). Such studies could help in quantifying the differences in carbon stock and hence the emission from conversion (Maraseni et al., 2008). These studies, however, have utilised field plots to estimate biomass and infer the stock for the whole study site. This approach is sufficient only for a few hectares, but costly and slow if implemented over large areas. It is also difficult to implement in remote and treacherous portions in a larger landscape. The use of satellite remote sensing techniques offers cost and time advantages in implementing large-scale biomass assessment. For this approach, remote sensing-based biomass assessment utilises the relationships between field-measured biomass data, imagery and other thematic maps to develop models that predict biomass in different locations of the study site. The outcome of remote sensing-based biomass estimation is a spatially-explicit pattern of the total above-ground biomass and its variations for the entire area (Samalca, 2007).

Satellite image-based biomass prediction models can be derived from radar backscatter polarisations, multispectral bands, vegetation index [e.g. Normalised Difference Vegetation Index (NDVI)], and vegetation cover biophysical variables [e.g. Leaf Area Index (LAI)]. These models can be developed with or without ancillary thematic map data (e.g. elevation; Lu et al., 2004; Simard et al., 2006; Fatoyinbo et al., 2008; Kumar et al., 2012; Sarker et al., 2012; Jachowski et al., 2013; Dube and Mutanga, 2015, 2016; Dusseux et al., 2015). In the tropics, however, during the rainy season where clouds are persistent, the use of multispectral image is challenging. In contrast, data from space-borne synthetic aperture radar (SAR) sensors are independent of daytime and weather conditions, and can provide valuable data for the monitoring of land cover.

Previous satellite remote sensing-based biomass retrieval and mapping studies in coastal areas have dealt mostly on mangrove forest alone (Simard et al., 2006; Proisy et al., 2007; Fatoyinbo et al., 2008; Jachowski et al., 2013; Kovacs et al., 2013; Aslan et al., 2016; Pham and Brabyn, 2017), and did not cover the land uses that replaced mangroves. This gap could be an important basis for productivity quantification and comparison with original land use. Simard et al. (2006) utilised SRTM elevation data to map the height of mangroves in the Everglades using linear regression with field data and used that mangrove height map and a local mangrove tree height-biomass equation to eventually map the biomass of mangrove therein. Proisy et al. (2007) used high-resolution IKONOS imagery and field data, and employed Fourier-based textural

ordination from canopy grain analysis to model and map the mangrove biomass in French Guiana. Fatoyinbo et al. (2008) also used SRTM elevation data and field data to map the mangrove height in Mozambique using linear regression and applied a general mangrove height-biomass equation to map the mangrove biomass in the area. In contrast, Jachowski et al. (2013) made use of high-resolution GeoEye-1 imagery and field data to estimate and map the biomass mangroves in Thailand using a suite of machine learning algorithm. Aslan et al. (2016) also used SRTM elevation and field data to map the mangrove height in Indonesia using linear regression but utilised non-linear quartile regression to generate biomass map of mangroves in the area using the mangrove height map and field biomass. More recently, Pham and Brabyn (2017) used SPOT images and object-based approach in combination with machine learning algorithms to estimate the biomass change of a mangrove forest in Vietnam.

The recent launch of the new-generation Sentinel-1 (SAR) and Sentinel-2 (multispectral) satellite missions of the Copernicus program of the European Space Station is expected to provide new capabilities for monitoring and mapping of biomass in the coastal zone of the tropics. Sentinel-1 provides radar imagery with HH+HV or VV+VH polarisations in C-band (Sentinel-1 Team, 2013) while Sentinel-2 offers 13 multispectral bands, including three vegetation red edge bands and two infrared bands, in addition to visible and near infrared bands (Sentinel-2 Team, 2015). However, to our knowledge, the retrieval and mapping of the biomass of mangrove forest and land uses that replaced them from data acquired by these newly launched multispectral and SAR instruments onboard the Sentinel-1 and Sentinel-2 satellite missions have not been reported yet in the scientific literature. Therefore, pioneering studies are needed to assess these new-generation satellite imagery.

In this study, we evaluated the ability of data from Sentinel-1 and Sentinel-2 imagery for the retrieval and predictive mapping of above-ground biomass of mangroves and the associated replacement land uses in a coastal area in the tropics. The specific objectives of the study included the following: (1) to determine and model the relationship between field-measured above-ground biomass and Sentinel-1 SAR backscatter coefficients and Sentinel-2 multispectral reflectance from mangrove forest and replacement non-forest land uses, (2) to evaluate the accuracy of the biomass prediction models, and (3) to evaluate the accuracy of the output predictive biomass maps. We developed and evaluated above-ground biomass models and predictive maps derived from Sentinel-1 SAR imagery, Sentinel-2 multispectral bands, Sentinel-2-derived vegetation indices (e.g. NDVI) and Sentinel-2-derived vegetation biophysical variables (e.g. LAI). The novelty of this paper is the use of Sentinel-1 and Sentinel-2 imagery in the estimation and mapping of the biomass of mangrove forests and non-forest land uses that replaced mangroves. This study attempted to contribute in developing remote sensing-based biomass predictive mapping techniques for mangrove area. It is a pioneering study that utilised Sentinel-1 SAR and Sentinel-2 optical data for biomass modelling and mapping of mangrove forests and non-forest land uses that replaced mangroves in tropical areas.

2. Methods

2.1. Study site

The study site is situated on the southern coast of Honda Bay within the administrative jurisdiction of Puerto Princesa City in the island province of Palawan, Philippines. It is geographically located between latitude 9.8028° to 9.9612°N and longitude 118.725° to 118.805°E (Fig. 1). The city is located in the central part of the province and is approximately 567 km south-west of Manila,

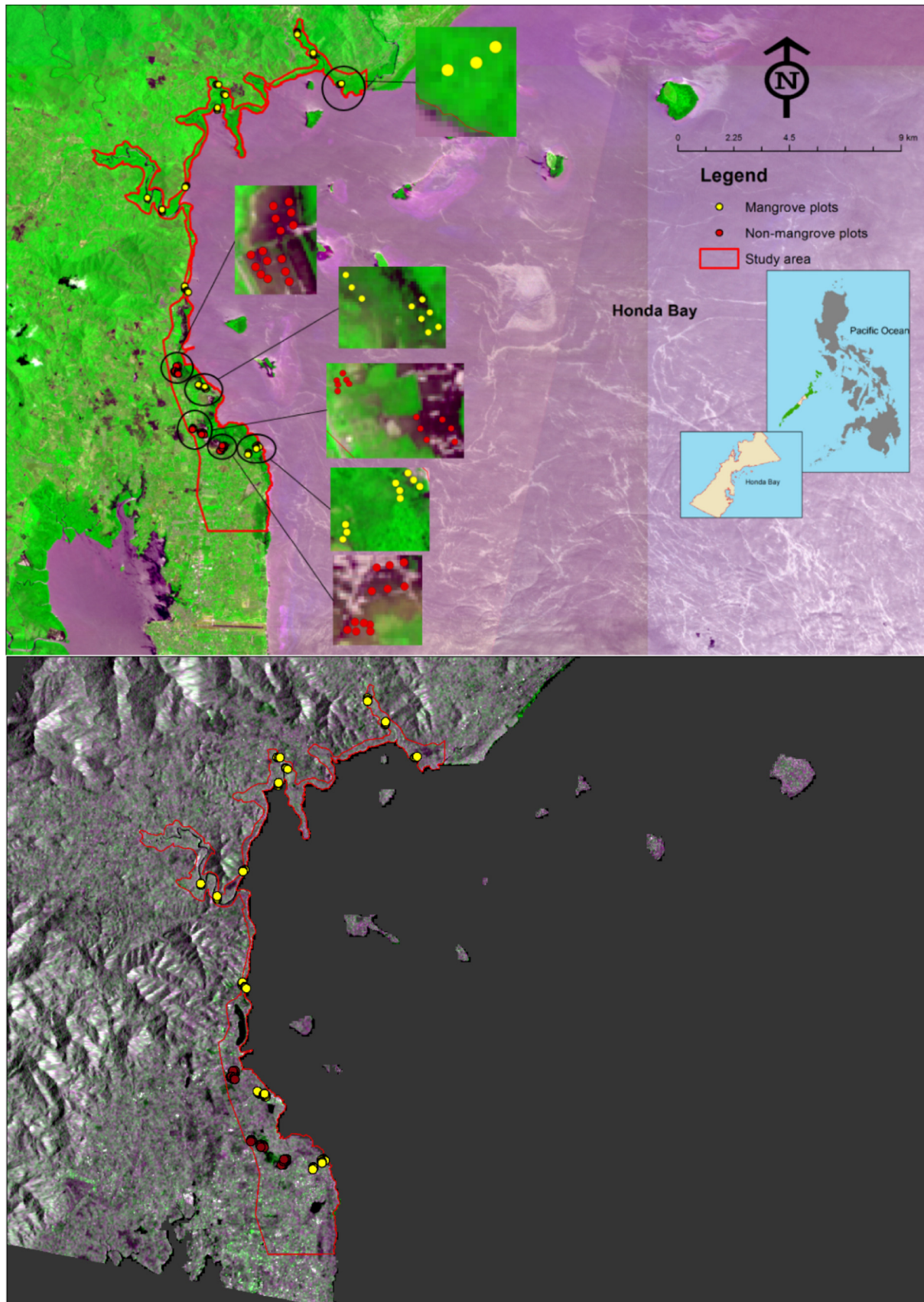


Fig. 1. Sample sentinel images used in the study. Top image: Sentinel-2 multispectral image acquired on April 2016 in false colour composite (RGB = R, NIR, B). Bottom image: Sentinel-1 SAR image acquired on October 2015 (RGB = VV, VH, VV in dB). Yellow and red dots are sampling plots. Inset maps: 1. Philippine map showing the relative location of Palawan province (green) with Puerto Princesa City at its midsection (beige); 2. Puerto Princesa map showing the Honda Bay area. (For interpretation of the references to colour in this figure legend, the reader is referred to the web version of this article.)

the country's capital. The climate in the study site is tropical, with two seasons (dry and wet) and under Type 3 based on Modified Corona's Climate Classification (i.e. no very pronounced maximum rain period, with one to three months only of dry season). The city receives an average annual rainfall of 1527.3 mm. Rainfall is highest during the months of October (216.1 mm) to November (211 mm) and lowest from January to April (less than 55 mm), with February (23.7 mm) as the driest month (23.7 mm of rain). Rainfall from May to September and December is at least 150 mm (PAGASA, 2016).

The southern coast of Honda Bay is presently a mosaic of a long band of mangrove forests interrupted by non-forest land uses such as agriculture, aquaculture, and built-up areas/settlements. Rivers in varying lengths dissect the mangrove forests, with both estuarine and fringing types. Mangroves, especially in the northern part of the study site, are extensive. The mangrove forests in the area are dominated mostly by the genus *Rhizophora* and can generally be classified as either closed canopy and open canopy stands. The former are dense, intact mangrove vegetation, with no significant open spaces or gaps inside, and are located mostly in areas far from roads and built-up areas. The open canopy mangroves, on the other hand, have open spaces, with lower tree density, with fresh stumps and cut branches. They are mostly near the aquaculture ponds, roads and built-up areas. The closed canopy mangroves that we sampled have a mean Leaf Area Index (LAI) of 2.25 and canopy gap fraction of 14% (~86% canopy foliage cover), respectively, as measured from *CI-110 Plant Canopy Imager* (CID Bio-Science, Washington, USA). One of the closed canopy mangroves that we sampled was once commercially logged in the 1980s and since then was allowed to re-grow and protected by the community. In contrast, the open canopy mangroves that we sampled had a mean LAI of 0.62 and canopy gap fraction of 64% (~36% canopy foliage cover).

In contrast, the non-forest land uses were historically occupied by mangroves prior to their conversion. The aquaculture ponds and salt ponds were mangrove forests until they were cleared in the early 1990s and were in operation until their abandonments in the early 2000s. The coconut plantation is a 20-year-old stand planted at the back of an open canopy mangrove forest and not actively managed as evidenced by the proliferation of dried leaves and fruits. The cleared mangrove is a deforested mangrove area that was gradually cleared from 2005 to 2008 but remained unutilised. The elevation of study plots that were established for data collection in the study site ranges from 1 m to 15 m. About 97% of the plots have elevations of 10 m and below. The study site has an area of 2749 ha, of which ca. 1216 ha is covered by mangrove forest, both under closed and open canopies.

2.2. Field data

The data was gathered from five coastal land uses, i.e. mangrove forest (closed canopy and open canopy), abandoned aquaculture pond, coconut plantation, abandoned salt pond, and cleared mangrove. The non-forest land uses were previously occupied by mangroves. In each land use, three sites were taken randomly for biomass measurements. However, due to access restriction and availability, the coconut plantation, salt pond and cleared mangroves have only one site each. Circular plots with 7 m in radii, established along line transects, were used in each land use to collect plot data necessary to estimate the biomass of each tree in a plot. For mangrove forest, three transects were established at each site (except for one open canopy mangrove which had only two transects due to thin cover). Each transect has three circular plots spaced 50 m apart. For non-forest land uses, two transects were established at each site except for salt pond which had three. Each transect also had three circular plots established about 25 m apart. At each plot, all the measurements (e.g. tree diameter) necessary to

determine the biomass were undertaken, following the method of Kauffman and Donato (2012) for biomass stock accounting. In each plot, geographic coordinates were recorded using a *Garmin* handheld GPS receiver. In total, 90 plots were established, of which 51 plots were in mangrove forests, 18 plots in the abandoned aquaculture ponds, nine plots in the abandoned salt pond and six plots each for coconut and cleared mangrove areas. In each plot, we measured all individuals at breast height (1.3 m from the ground) or 30 cm above the highest prop root for stilt-rooted species like *Rhizophora* spp. Allometric equations were used to compute for the aboveground biomass of each individual.

$$\text{Biomass(kg)} = 0.251 * \rho * D^{2.46} \quad (1)$$

$$\text{Biomass(kg)} = 0.186D^{2.31} \quad (2)$$

$$\text{Biomass(kg)} = 0.168D^{2.42} \quad (3)$$

$$\text{Biomass(kg)} = 0.235D^{2.42} + \text{Biomass}_{\text{stilt}}(\text{kg}) = 0.0209D^{2.55} \quad (4)$$

$$\text{Biomass(kg)} = 0.7854 * D^2 * H * \rho * 1.6 \quad (5)$$

Eq. (1), from Komiyama et al. (2005), was used for eight species (*Aegiceras floridum*, *Sonneratia alba*, *Xylocarpus moluccensis*, *X. granatum*, *Campostemon philippinense*, *Ceriops tagal*, *Heritiera littoralis* and *Lumnitzera racemosa*). Eqs. (2) and (3) were from Clough and Scott (1989) and were used for *Bruguiera gymnorhiza*, and *B. parviflora* and *B. sexangula*, respectively. Eq. (4) was from Ong et al. (2004) and used for *Rhizophora apiculata*, *R. mucronata*, and *R. stylosa*, while Eq. (5) was from Brown (1997) and used for coconut.

In summary, the mangrove forests were dominated by *Rhizophora apiculata* and *R. mucronata*. In the abandoned aquaculture pond, individuals of *R. apiculata* and *Ceriops tagal* were also encountered. The tree density in the mangroves averaged 1260 trees per hectare. In the land uses that replaced mangroves such as coconut, the tree density was only 195 per hectare while it was only 40 trees per hectare in aquaculture pond. Trees were absent in both the abandoned salt pond and cleared mangrove. Furthermore, the average above-ground biomass of mangrove was 65.1 Mg ha^{-1} (range: 1.1 – 210 Mg ha^{-1}). In contrast, the average above-ground biomass in the coconut plantation was only 11.4 Mg ha^{-1} (range: 0.2 – 19.7 Mg ha^{-1}) and 0.04 Mg ha^{-1} (range: 0 – 0.40 Mg ha^{-1}) in the abandoned aquaculture pond. Fig. 2 shows the profile of the above-ground biomass in the 90 study plots. Mangroves were in plots 1 to 51, aquaculture ponds were in plots 52 to 69, coconut plantations were in plots 70 to 75, salt ponds in plots 76 to 84 and cleared mangroves in plots 85 to 90. Biomass in abandoned aquaculture pond ranged from zero to negligible, while there was no vegetation present in the abandoned salt pond and cleared mangrove.

2.3. Satellite data collection and pre-processing

This study used data from Sentinel-1 (Synthetic Aperture Radar) and Sentinel-2 (Multispectral) imagery of the European Space Agency downloaded from the agency's Copernicus Sentinels Scientific Data Hub (ESA, 2016). The list of Sentinel images used for the study is presented in Table 1. The acquired Sentinel-1 C-band (5.405 GHz) images were collected in Interferometric Wide Swath mode with a swath width of 250 km, of VH (Vertical transmit – Horizontal receive) and VV (Vertical transmit – Vertical receive) polarisations, and in high-resolution (HR) Level-1 Ground Range Detected (GRD) processing level. The images are already multi-looked (5×1) and with a pixel size of 10 m (Sentinel-1 Team, 2013). The collected Sentinel-2 data, on the other hand, is an orthorectified, top-of-atmosphere reflectance (Level 1C), 100 km

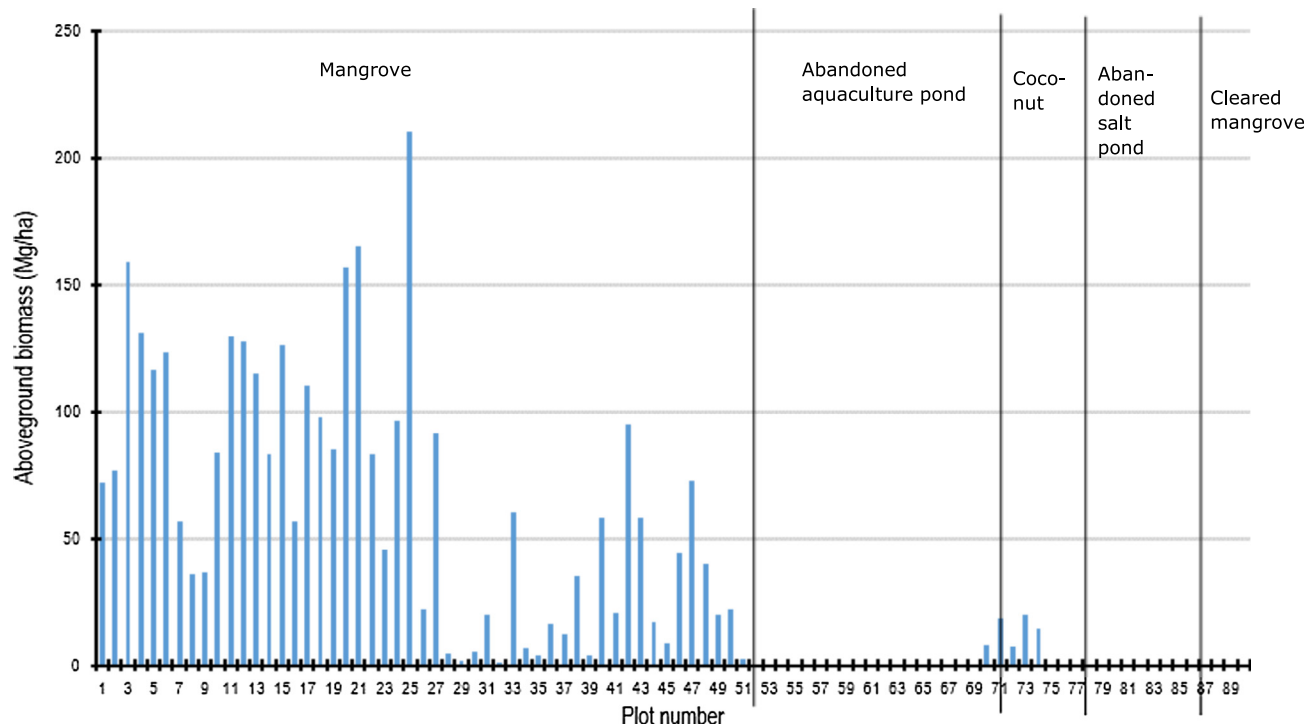


Fig. 2. Field plots profile of above-ground biomass in the study site. Plots 1 to 51 are mangrove plots, 52 to 69 are abandoned aquaculture pond plots, 70 to 75 are coconut plantation plots, 76 to 84 are abandoned salt pond plots, and 85 to 90 are cleared mangrove plots.

Table 1
List of Sentinel imagery acquired for the study.

Mission	Product	Observation date	Cell size (m)	Swath width (km)
Sentinel-1A	Level-1GRD-HR	October 31, 2015	10	250
Sentinel-1A	Level-1 GRD-HR	December 30, 2015	10	250
Sentinel-1A	Level-1 GRD-HR	January 11, 2016	10	250
Sentinel-2A	Multispectral image Level-1C	April 11, 2016	10	100

× 100 km image in UTM/WGS84 projection, with 13 spectral bands in the visible, near infrared and short-wave infrared regions. The imagery is in 10 m (4 bands), 20 m (6 bands) and 60 m (3 bands) spatial resolutions. Accordingly, the Level-1C product has been processed for radiometric and geometric corrections including orthorectification and spatial registration on a global reference system (Sentinel-2 Team, 2015). In addition, elevation data (1-arc second, ~30 m) from SRTM product was acquired from the United States Geological Service's Earth Explorer (USGS, 2016) for inclusion in the analysis of the Sentinel data.

A flowchart of data processing steps used in the study is summarised in Fig. 2. The software SNAP (Sentinel's Application Platform) version 4.0 of the European Space Agency was used to pre-process the Sentinel-1, Sentinel-2 and elevation data. The pre-processing steps for the acquired Sentinel-1 SAR data adopted the Sentinel-1 Toolbox pre-processing steps described by Veci (2015) for multi-look SAR image. It consisted of (1) image calibration; (2) speckle reduction, and (3) terrain correction. Image calibration radiometrically corrects the SAR image pixel value into one that represents the radar backscatter of the reflecting surface, as well as correction for incidence angle effect and replica pulse power variation. This process converts the pixel values of the SAR image into radar intensity backscatter coefficient (σ^0). Furthermore, speckle reduction using Refined Lee Filter was done to reduce the speckle effect in the image to allow better backscatter analysis and interpretation. Finally, terrain correction was performed using the Range-Doppler Terrain Correction

to reproject the SAR image into a map projection (Veci, 2015; Liu, 2016).

For the optical Sentinel-2 image, the acquired Level-1C orthorectified, top-of-atmosphere image was atmospherically corrected and processed to Level-2A product to obtain bottom-of-atmosphere corrected reflectance image. This was also done in SNAP software using the recent radiative transfer model-based SEN2COR atmospheric correction processor (version 2.2.1). The pre-processed Sentinel images, as well as the elevation data, were brought into a common map projection (i.e. UTM Zone 50 WGS84) and resampled to 10m pixel size. Subsetting was done each for the Sentinel SAR and multispectral images and the SRTM DEM to reduce the image size and the processing time, and to cover only the general area along the coast of Honda Bay.

2.4. Modelling the relationship between field biomass and satellite data

We divided the Sentinel imagery data into four predictor groups of biomass: (a) multi-date SAR raw channels (Fig. 3), (b) multispectral bands, (c) derived Vegetation Indices, and (d) derived biophysical variables. Thus, modelling the relationship of Sentinel image data and field measured biomass was done in four parts (Table 2). The first part consisted of relating the field data with Sentinel SAR polarisation channels (i.e. VH and VV) and their combination. The second part proceeded with relating the field biomass with Sentinel 2 multispectral bands and their combination. The third part

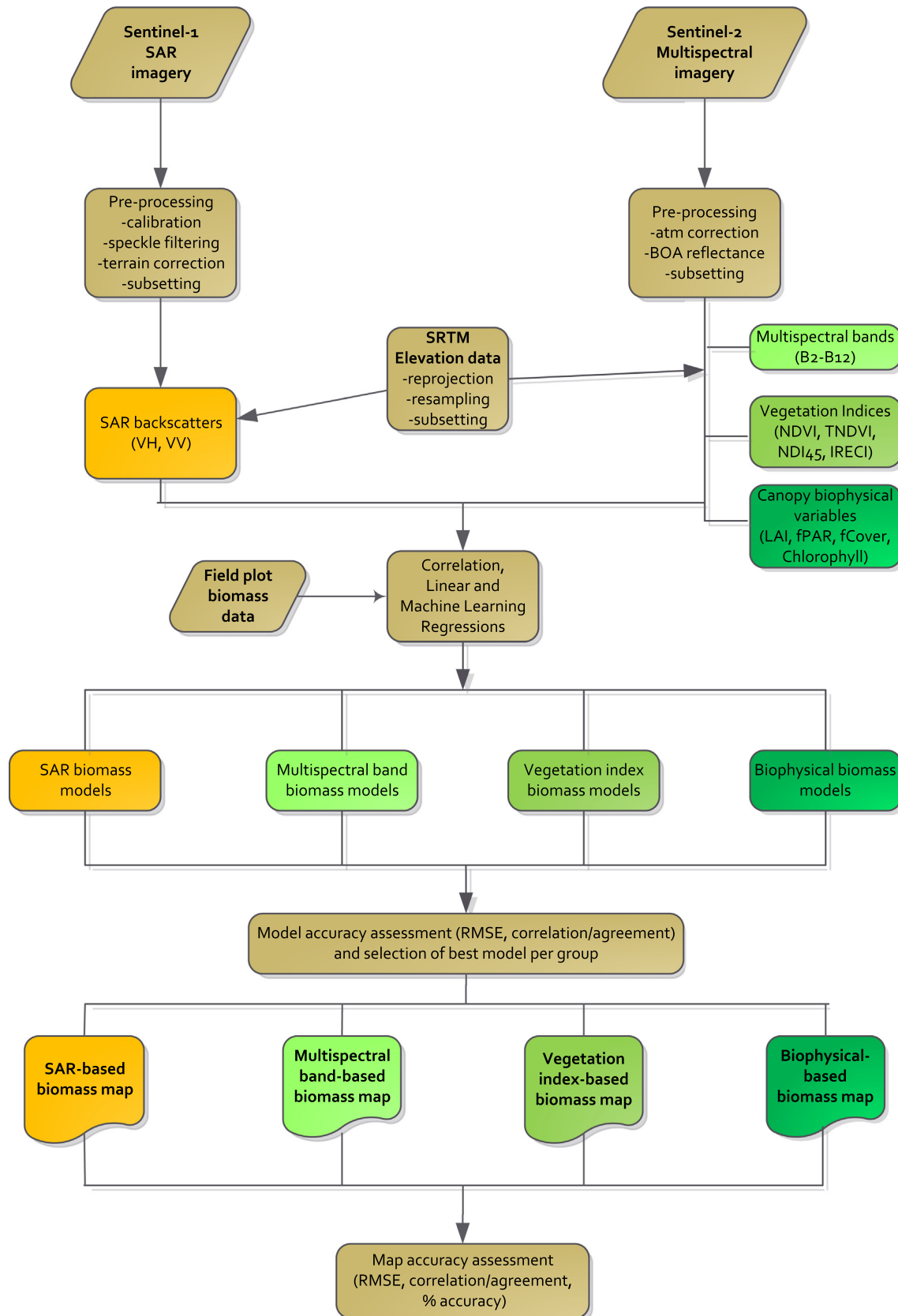


Fig. 3. Flowchart of steps used for the aboveground biomass retrieval and mapping of mangrove forests and their non-forest replacement land uses using the Sentinel SAR and multispectral imagery. There were four Sentinel groups considered in the study: 1. SAR-based group, 2. Multispectral band-based group, 3. Vegetation indices-based group, and 4. Vegetation biophysical variables-based group.

Table 2

Sentinel-based imagery data predictors of above-ground biomass including space-borne elevation data.

Group	Source image	Predictor variable	Relevant channel/band/index	Definition
1	Sentinel-1	Polarisation/channel	VH-Oct	VH channel (dB) for October 2015
			VV-Oct	VV channel (dB) for October 2015
			VH-Dec	VH channel (dB) for December 2015
			VV-Dec	VV channel (dB) for December 2015
			VH-Jan	VH channel (dB) for January 2016
			VV-Jan	VV channel (dB) for January 2016
2	Sentinel-2	Multispectral Bands	Band 2	Blue, 490 nm
			Band 3	Green, 560 nm
			Band 4	Red, 665 nm
			Band 5	Red edge, 705 nm
			Band 6	Red edge, 749 nm
			Band 7	Red edge, 783 nm
			Band 8	Near Infrared, 842 nm
			Band 8a	Near Infrared, 865 nm
			Band 11	Short Wave IR, 1610 nm
			Band 12	Short Wave IR, 2190 nm
			NDVI	(Band 8 – Band 4)/(Band 8 + Band 4) [*]
			NDI45	(Band 5 – Band 4)/(Band 5 + Band 4) ^{**}
3	Sentinel-2	Vegetation indices	IRECI	(Band 7 – Band 4)/(Band 5/Band 6) ^{***}
			TNDVI	[(Band 8 – Band 4)/(Band 8 + Band 4) + 0.5] ^{1/2****}
4	Sentinel-2	Vegetation biophysical variables	LAI	Leaf Area Index
			fCover	Fraction of Vegetation Cover
			fPAR	Fraction of Absorbed Photosynthetically Active Radiation
			Cab	Chlorophyll content in the leaf
1 to 4	SRTM DEM	Elevation		Elevation, 30 m resolution

IRECI = Inverted Red-Edge Chlorophyll Index; TNDVI = Transformed Normalised Difference Vegetation Index.

* Rouse et al. 1973 as cited in [SNAP \(2016\)](#).

** Delegido et al. 2011 as cited in [SNAP \(2016\)](#).

*** Clevers et al. 2000 as cited in [SNAP \(2016\)](#).

**** Senseman et al. 1996 as cited in [SNAP \(2016\)](#).

involved relating the field biomass with Sentinel-2-derived vegetation indices like Normalised Difference Vegetation Index (NDVI) and Normalised Difference Index (NDI45). The last part used Sentinel-2-derived vegetation cover biophysical measures such as Leaf Area Index (LAI) and Fraction of Absorbed Photosynthetically Active Radiation (fPAR), among other variables. We supplemented the Sentinel backscatter and reflectance data with elevation data from SRTM DEM to assess whether the inclusion of elevation can improve the biomass prediction. All modelling tasks were implemented using IBM SPSS Statistics version 23 (IBM, USA) and the Waikato Environment for Knowledge Analysis (WEKA, version 3.8.0, The University of Waikato, NZ). The WEKA software is a collection of machine learning algorithms ([Hall et al., 2009](#)).

LAI and other biophysical cover variables (see [Table 2](#)) were also derived in SNAP from its biophysical processor that uses neural network algorithm ([SNAP, 2016](#)) based on PROSAIL radiative transfer model ([Jacquemoud et al., 2009](#)). The retrieval of these biophysical variables was also done for the SPOT image by [Dusseux et al. \(2015\)](#). The model was prepared using the entire dataset. The dataset was first subjected to linear regression. This process steps through the variables, removing the one with the smallest standardised coefficient until no improvement was observed in the estimate of the error (as given by the Akaike Information Criterion (AIC)), eliminating collinear variable/s. To assess the model performance, a leave-one-out approach with 90-fold cross-validation was performed to compute the prediction error (Root Mean Square Error (RMSE)) and correlation coefficient/agreement (r) between the observed and predicted data. In the leave-one-out approach, each sample was excluded one by one while the model is trained with the remaining samples to predict the excluded sample.

To assess if the correlation with biomass and prediction error from the linear models can still be improved, the set of predictors from the linear models with the highest r and lowest RMSE for

each part was further subjected to 17 machine learning algorithms available in the WEKA machine learning software ([Table 3](#)). The model/algorithm with highest r and lowest RMSE was selected for use in predictive mapping of biomass which was implemented in ArcGIS (version 10.3.1, ESRI, USA). Four biomass predictive maps were produced which were derived from Sentinel-1 SAR channels, Sentinel-2 bands, Sentinel-2 vegetation index, and Sentinel-2 vegetation biophysical variable.

Table 3

Machine learning algorithms used in the study. These algorithms are available from WEKA machine learning software ([Hall et al., 2009](#)).

Algorithm	Classifier type	Key description
ElasticNet	Functions	Coordinate descent-based regression for 'elastic net'-related problem
GaussianProcesses	Functions	Gaussian processes for regression
IsotonicRegression	Functions	Learns an isotonic regression model
LeastMedSq	Functions	Least median squared linear regression
MultilayerPerceptron	Functions	Backpropagation to classify instances
PaceRegression	Functions	Pace regression linear models
RBFNetwork	Functions	Normalized Gaussian radial basis function network.
RBFRegressor	Functions	Supervised Radial basis function networks
SMOreg	Functions	Support vector machine for regression
AlternatingModelTree	Trees	An alternating model tree by minimising squared error
DecisionStump	Trees	Building and using a decision stump
RandomForest	Trees	Construction a forest of random trees
RandomTree	Trees	Tree construction based on K-randomly chosen attributes
REPTree	Trees	Fast decision tree learner
IBk	Lazy	K-nearest neighbour classifier
KStar	Lazy	Instance-based classifier
LWL	Lazy	Locally weighted learning

The accuracy of the predicted maps was assessed for their overall RMSE, agreement/correlation coefficient (r) between predicted and observed values, and map accuracy (%) based on the range value of the dataset (Christensen et al., 2004). Extraction of the pixel value of the 90 plots for each of the four predictive maps was done using ArcGIS. The prediction errors (RMSE) were also computed for each land use in each Sentinel image-derived map.

3. Results

3.1. Relationship of field biomass and sentinel image data, and model assessment

3.1.1. Sentinel-1 (SAR) polarisations

There was an increase in the backscatter values as the above-ground biomass increases, i.e. from nil in aquaculture pond, salt pond and cleared mangrove to low biomass in the coconut plantation, and low to high biomass in mangroves (Fig. 4). Backscatter (dB) values of vegetated mangrove and coconuts were comparable, -13.41 and -13.19 in VH polarisation and -7.51 and -7.86 in VV polarisation, respectively. Non-vegetated areas under aquaculture pond, salt pond and cleared mangrove had lower backscatter value (dB) in VH polarisation (i.e. -18.098 for aquaculture pond, -19.80 for salt pond and -16.16 for cleared mangrove). For VV polarisation, the trend was less clear for non-vegetated areas, with lower backscatter value of -9.22 and -10.77 for aquaculture pond and salt pond, but higher backscatter for cleared mangrove of -6.83 .

Single-date VH channel had better correlations with biomass ($r = 0.48\text{--}0.51$ vs. $r = 0.28\text{--}0.45$) than VV polarisation. The multi-date combination of VH and VV polarisations had a higher correlation with biomass than single date imagery, albeit the relationship is

only moderate ($r = 0.55$). However, when elevation was added to multi-date VH-VV channels, the relationship with biomass was greatly improved ($r = 0.84$). This model was able to explain 69% of the biomass variability and had the lowest prediction error of 28.36 Mg ha^{-1} , among the SAR models evaluated (Table 4).

3.1.2. Sentinel-2 multispectral bands and combination

Figs. 5 and 6 present the reflectance in the visible, red edge and infrared bands in relation to the above-ground biomass of mangroves and the non-forest land uses that replaced them. Bands in the Red edge 2, Red edge 3, and Near-infrared have better correlations ($r = 0.69$ to 0.72) with above-ground biomass than bands in the visible and short-wave infrared regions. Band combination of Red edge1 and Red edge2, as well as NIR and SWIR2 bands, had stronger and better correlations with above-ground biomass than individual bands and other band combinations. However, the inclusion of elevation with band combination of Red, Red edge 1, and Red edge3 greatly improved the correlation ($r = 0.84$). This band-elevation combination had the least prediction error (28 Mg ha^{-1} ; Table 4).

3.1.3. Sentinel-2-derived vegetation indices

Fig. 6 shows the plot profile of vegetation indices in the study site. Indices close to zero for NDVI, IRECI and NDI45 were non-vegetated plots under aquaculture pond, salt pond and cleared mangrove, respectively. Among the Sentinel-derived vegetation indices included in this study, NDI45 and IRECI had the highest correlation ($r = 0.80$) to biomass. Adding elevation to the indices slightly improved the correlation, of which the highest was in IRECI and elevation combination ($r = 0.84$) as presented in Table 4. This combination also had the lowest prediction error of 28 Mg ha^{-1} .

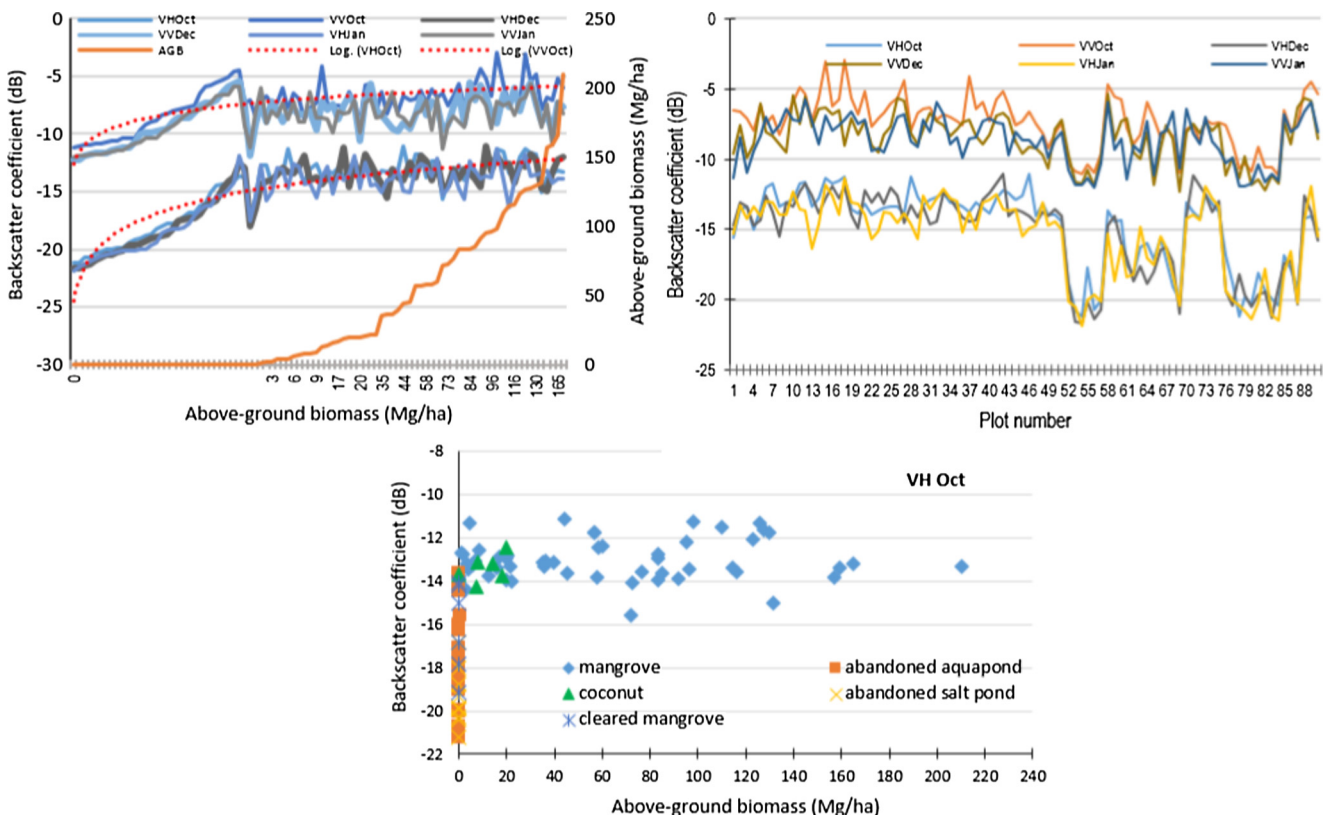


Fig. 4. Relationships of observed above-ground biomass and Sentinel-1 SAR backscatter coefficient (σ^0, dB) in the different study coastal land uses. Plots were arranged from nil to high biomass (top left), according to land use/plot number (top right) and in October 2015 for VH polarisation (bottom). Plots 1 to 51 (mangrove), 52 to 69 (abandoned aquaculture), 70 to 75 (coconut plantation), 76 to 84 (abandoned salt pond) and 85 to 90 (cleared mangrove).

Table 4

Correlation of observed above-ground biomass and Sentinel-based predictors.

Modelling group	Predictor/s	Correlation with biomass, r	p-value	Agreement/correlation of observed and predicted value, r	Model prediction error, RMSE (Mg ha^{-1})
1. Sentinel-1 (SAR) polarisation	VH Oct	0.50	<.001	0.47	44.16
	VV Oct	0.45	<.001	0.42	45.50
	VH Dec	0.51	<.001	0.49	43.67
	VV Dec	0.33	.001	0.28	48.03
	VH Jan	0.48	<.001	0.45	44.72
	VV Jan	0.28	.007	0.21	48.99
	VV Oct, VH Dec, VV Jan	0.55	<.001	0.47	44.33
	VV Oct, VH Jan, Elevation	0.84	<.001	0.82	28.36
2. Sentinel-2 (multispectral) bands	Blue	-0.57	<.001	0.53	42.40
	Green	-0.54	<.001	0.51	43.03
	Red	-0.65	<.001	0.63	38.74
	Red Edge 1	-0.50	<.001	0.47	44.16
	Red Edge 2	0.69	<.001	0.67	37.09
	Red Edge 3	0.72	<.001	0.71	35.34
	NIR	0.72	<.001	0.71	35.45
	NIRa	0.72	<.001	0.70	35.60
	SWIR 1	-0.42	<.001	0.38	46.23
	SWIR 2	-0.59	<.001	0.56	41.37
	NIR, SWIR 2	0.80	<.001	0.79	30.90
	Red, Red Edge 1	0.71	<.001	0.68	36.59
	Red, Red Edge 2	0.77	<.001	0.76	32.68
	Red Edge 1, Red Edge 2	0.79	<.001	0.77	31.83
	Red, red edge 1, NIR, Elevation	0.84	<.001	0.82	28.92
	Red, Red edge1, Red edge3, Elevation	0.84	<.001	0.82	28.47
3. Sentinel-2 derived vegetation indices	NDI45	0.80	<.001	0.79	30.74
	IRECI	0.80	<.001	0.79	30.73
	TNDVI	0.72	<.001	0.70	35.54
	NDVI	0.74	<.001	0.73	34.44
	NDI45, Elevation	0.84	<.001	0.82	28.83
	IRECI, Elevation	0.84	<.001	0.83	28.02
4. Sentinel-2 derived biophysical variables	LAI	0.80	<.001	0.79	30.91
	fPAR	0.77	<.001	0.75	32.89
	fCover	0.78	<.001	0.77	32.11
	Chlorophyll content	0.77	<.001	0.76	32.32
	LAI, Elevation	0.84	<.001	0.82	28.33
	Chlorophyll, Elevation	0.84	<.001	0.82	28.38

3.1.4. Sentinel-2-derived vegetation biophysical variables

The plot profile of the Sentinel-2-derived vegetation biophysical variables included in the study is also shown in Fig. 7. Non-vegetated areas under aquaculture pond, salt pond and cleared mangrove had values close to zero whereas vegetated areas under coconut had a lower value of vegetation cover (less than 0.5 on average) compared to mangroves. Leaf Area Index (LAI) had better correlation with biomass ($r = 0.80$) than the other vegetation cover variables evaluated (Table 4). Adding elevation data improved the correlation and reduced the error of prediction. The highest correlation with biomass and lowest prediction error was for the combination of LAI and elevation ($r = 0.84$; RMSE = 28.38 Mg ha^{-1}).

3.2. Linear regression versus machine learning algorithms

Compared to linear regression, the use of machine learning algorithms SMOreg and ElasticNet gave better biomass prediction from Sentinel-1 SAR and Sentinel-2-derived vegetation cover data, respectively. However, for Sentinel-2 band combination and Sentinel-2 derived vegetation index, linear regression gave better biomass prediction than the machine learning algorithms. Table 5 shows the evaluation of biomass prediction from machine learning algorithms and traditional linear regression in terms of the agreement of observed and predicted values as well as the prediction error.

3.3. Biomass predictive mapping

The model from the best algorithm (lowest RMSE and highest r) from each of the four biomass prediction groups was then used to

estimate and map the above-ground biomass (AGB) values throughout the study area, as shown in the equations below:

$$\begin{aligned} \text{Sentinel 1-derived AGB} = & -32.0684 + 1.7712 * \text{VVOct} \\ & - 1.8129 * \text{VHJan} + 12.6514 \\ & * \text{elevation} \end{aligned} \quad (6)$$

$$\begin{aligned} \text{Sentinel-2 bands-derived AGB} = & -9.3577 + 792.5243 * \text{Band 4} - 987.7312 * \text{Band 5} \\ & + 234.2441 * \text{Band 7} + 10.082 * \text{elevation} \end{aligned} \quad (7)$$

$$\begin{aligned} \text{Sentinel-2 vegetation index-derived AGB} = & -12.7514 + 36.0378 * \text{IRECI} + 8.0015 * \text{elevation} \end{aligned} \quad (8)$$

$$\begin{aligned} \text{Sentinel-2 vegetation cover-derived AGB} = & -16.067 + 7.474 * \text{LAI} + 9.296 * \text{elevation} \end{aligned} \quad (9)$$

Fig. 8 presents the biomass maps derived from Sentinel-1 SAR and Sentinel-2 multispectral images, in conjunction with SRTM elevation data. The spatial variation of predicted AGB conforms to those observed in the field. The predicted high biomass areas were in the northern part of the study site which is in agreement with the field observation where closed canopy mangrove forest can be found. Likewise, the lowest AGB estimates were found in the middle to southern part of the study site and consistent with field condition where non-forest land uses that replaced mangroves are usually found.

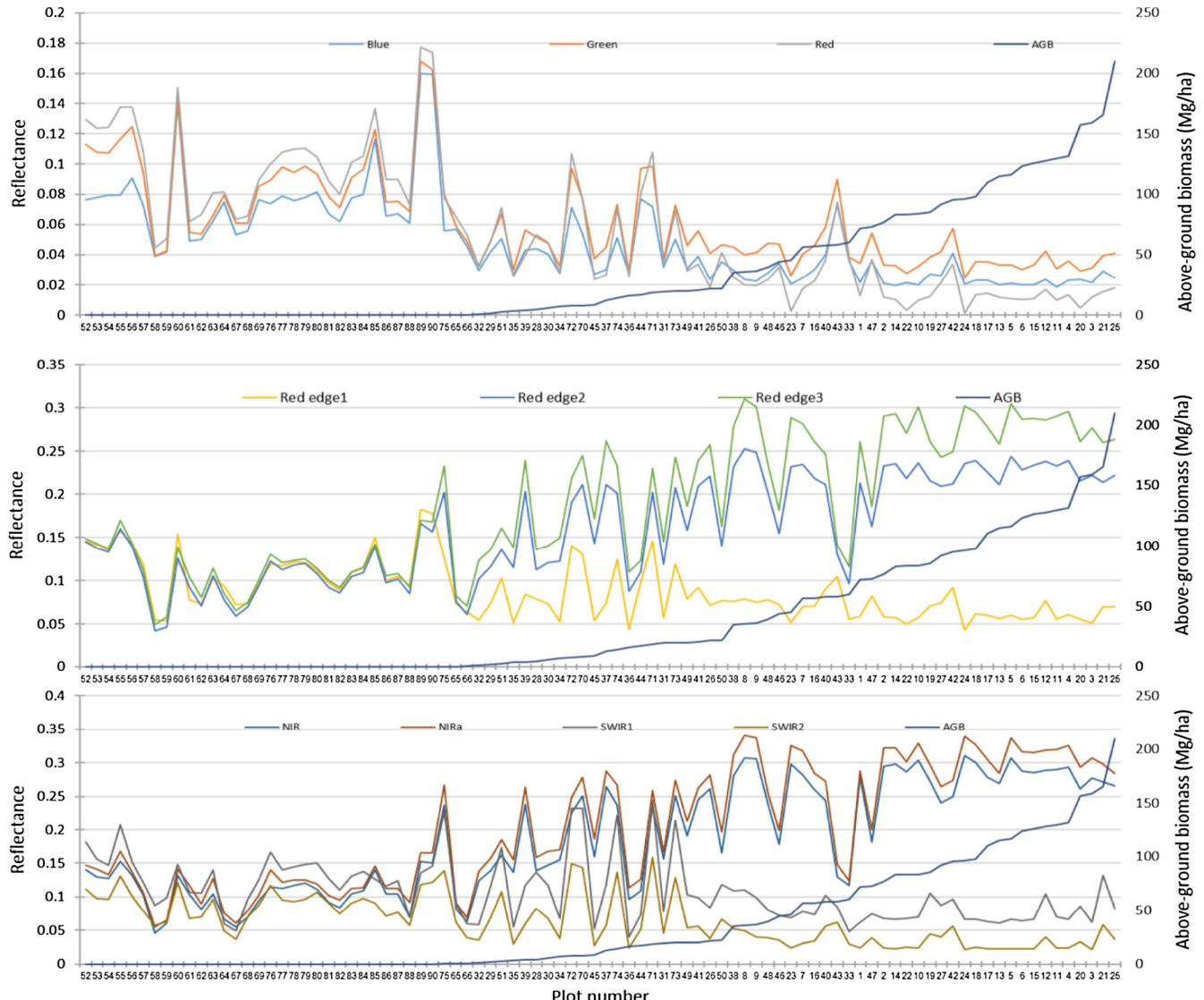


Fig. 5. Relationships of observed above-ground biomass with Sentinel-2 multispectral bands in the visible, red edge and infrared regions. Plots were arranged from nil to high biomass. Plots 1 to 51 (mangrove), 52 to 69 (abandoned aquaculture pond), 70 to 75 (coconut plantation), 76 to 84 (abandoned salt pond) and 85 to 90 (cleared mangrove).

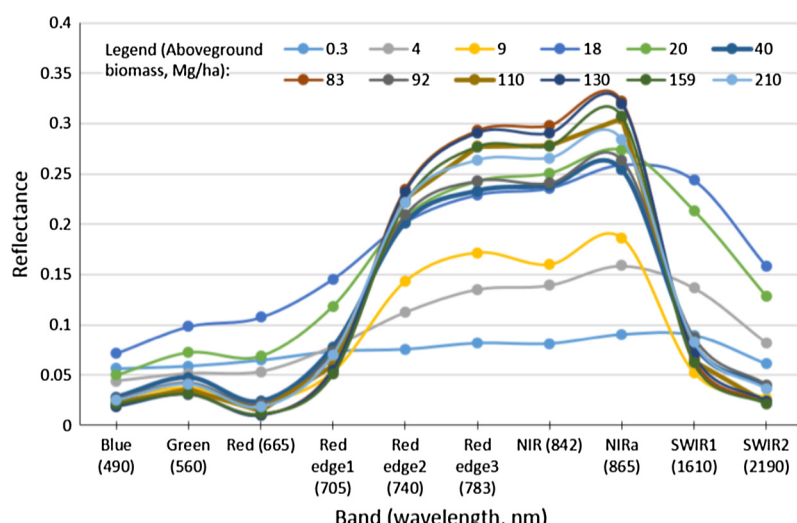


Fig. 6. Relationship of spectral bands and above-ground biomass.

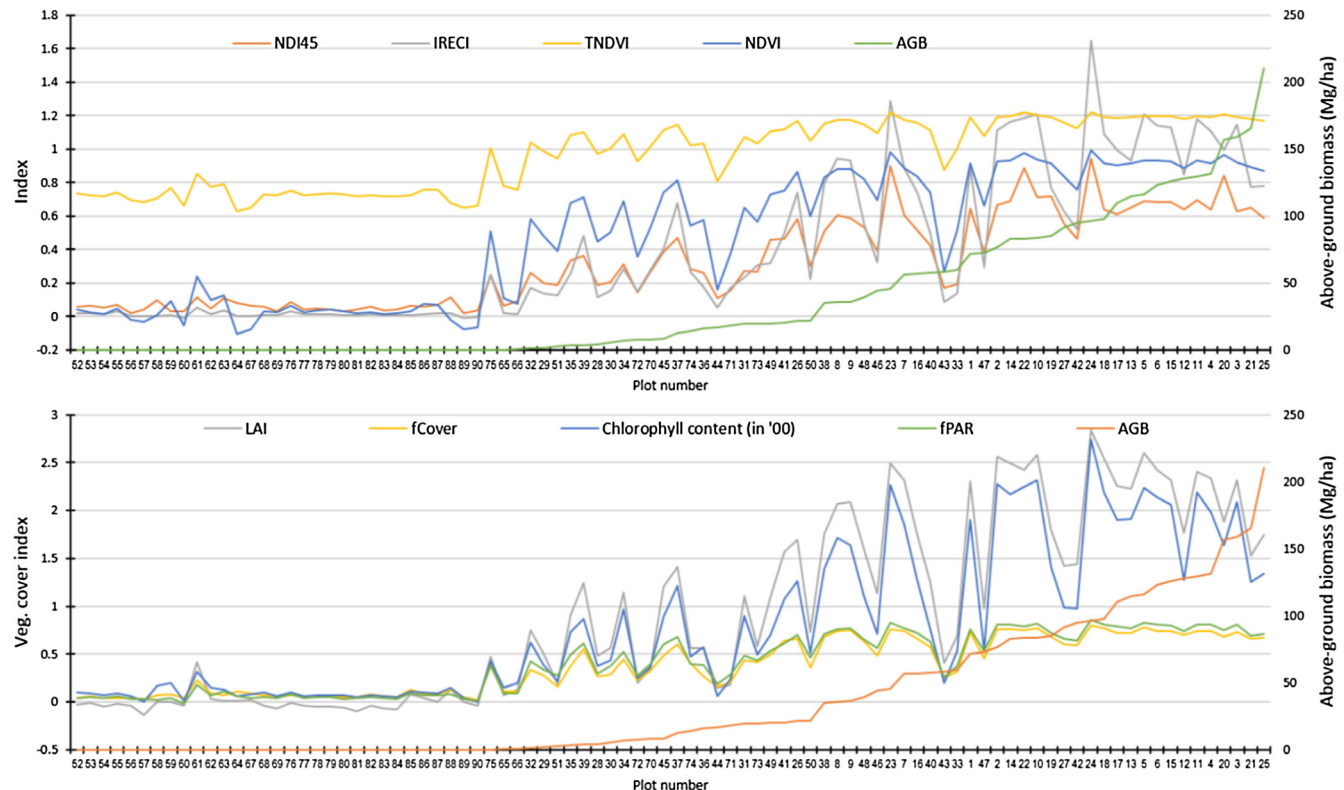


Fig. 7. Relationship of observed above-ground biomass with Sentinel-2-derived vegetation indices (top panel) and Sentinel-2-derived biophysical variables (bottom panel). Plots were arranged from nil to high biomass. Plots 1 to 51 (mangrove), 52 to 69 (abandoned aquaculture), 70 to 75 (coconut plantation), 76 to 84 (abandoned salt pond) and 85 to 90 (cleared mangrove).

Table 5

Algorithms used in the study and their accuracy evaluation for biomass prediction.

Algorithm	S-1 SAR		S-2 bands		S-2 veg. index		S-2 LAI	
	r	RMSE	r	RMSE	r	RMSE	r	RMSE
Linear Regression	0.82	28.36	0.82	28.47	0.83	28.02	0.82	28.33
ElasticNet	0.82	28.34	0.82	28.61	0.82	28.35	0.83	28.25
GaussianProcesses	0.78	33.23	0.78	31.35	0.82	41.14	0.81	41.64
IsotonicRegression	0.80	30.48	0.80	29.99	0.79	31.26	0.80	30.48
LeastMedSq	0.82	43.98	0.65	48.69	0.74	44.61	0.82	43.28
MultilayerPerceptron	0.77	32.98	0.76	33.33	0.78	31.86	0.78	31.90
PaceRegression	0.82	28.38	0.81	29.04	0.83	28.03	0.82	28.33
RBFNetwork	0.46	44.32	0.76	32.34	0.76	32.53	0.76	32.32
RBFRegressor	0.78	31.40	0.80	29.94	0.80	42.06	0.78	31.92
SMOreg	0.83	27.75	0.80	29.81	0.82	29.18	0.80	30.58
AlternatingModelTree	0.58	55.81	0.71	35.92	0.44	59.12	0.38	62.48
DecisionStump	0.71	35.58	0.73	34.40	0.67	37.64	0.70	36.05
RandomForest	0.76	32.95	0.75	33.81	0.75	33.71	0.72	35.13
RandomTree	0.54	48.75	0.65	42.42	0.67	41.17	0.61	43.15
REPTree	0.79	31.26	0.76	32.96	0.77	31.89	0.77	32.04
IBk	0.69	38.80	0.61	43.20	0.59	44.67	0.59	43.35
KStar	0.74	33.93	0.71	36.75	0.78	31.15	0.77	31.74
LWL	0.75	33.07	0.86	27.54	0.77	33.82	0.69	36.68

S-1 SAR = Sentinel 1 polarisation, S-2 bands = Sentinel 2 multispectral bands.

S2 veg. index = Sentinel 2-derived vegetation index, S2 LAI = Sentinel 2-derived Leaf Area Index.

r = correlation/agreement of observed and predicted values, RMSE = Root Mean Square Error (Mg ha^{-1}).

The accuracy assessment (Fig. 9) of the Sentinel-based predicted biomass maps revealed that their prediction error (RMSE) values were almost similar (range: $28.05\text{--}30.92 \text{ Mg ha}^{-1}$), but lowest in Sentinel-2-LAI-derived biomass map and highest in Sentinel-2 optical bands-derived map. The overall map accuracy ranged from 85.3% (Sentinel-2 optical bands-based map) to 86.6% (Sentinel-2-derived LAI-based map). Correlation coefficient/agreement (r) between measured and predicted biomass were all signif-

icant at 0.01 level and computed at 0.84, 0.82, 0.83 and 0.84 for models derived from Sentinel SAR-, Sentinel-2 multispectral bands, Sentinel-2 IRECI vegetation index and Sentinel-2 LAI datasets, respectively. There was no significant difference between the observed and predicted biomass values for each of the biomass map based on paired t-tests ($p > .05$).

Also, among the land uses, the prediction errors for mangrove forest were similar for the four Sentinel-derived biomass maps

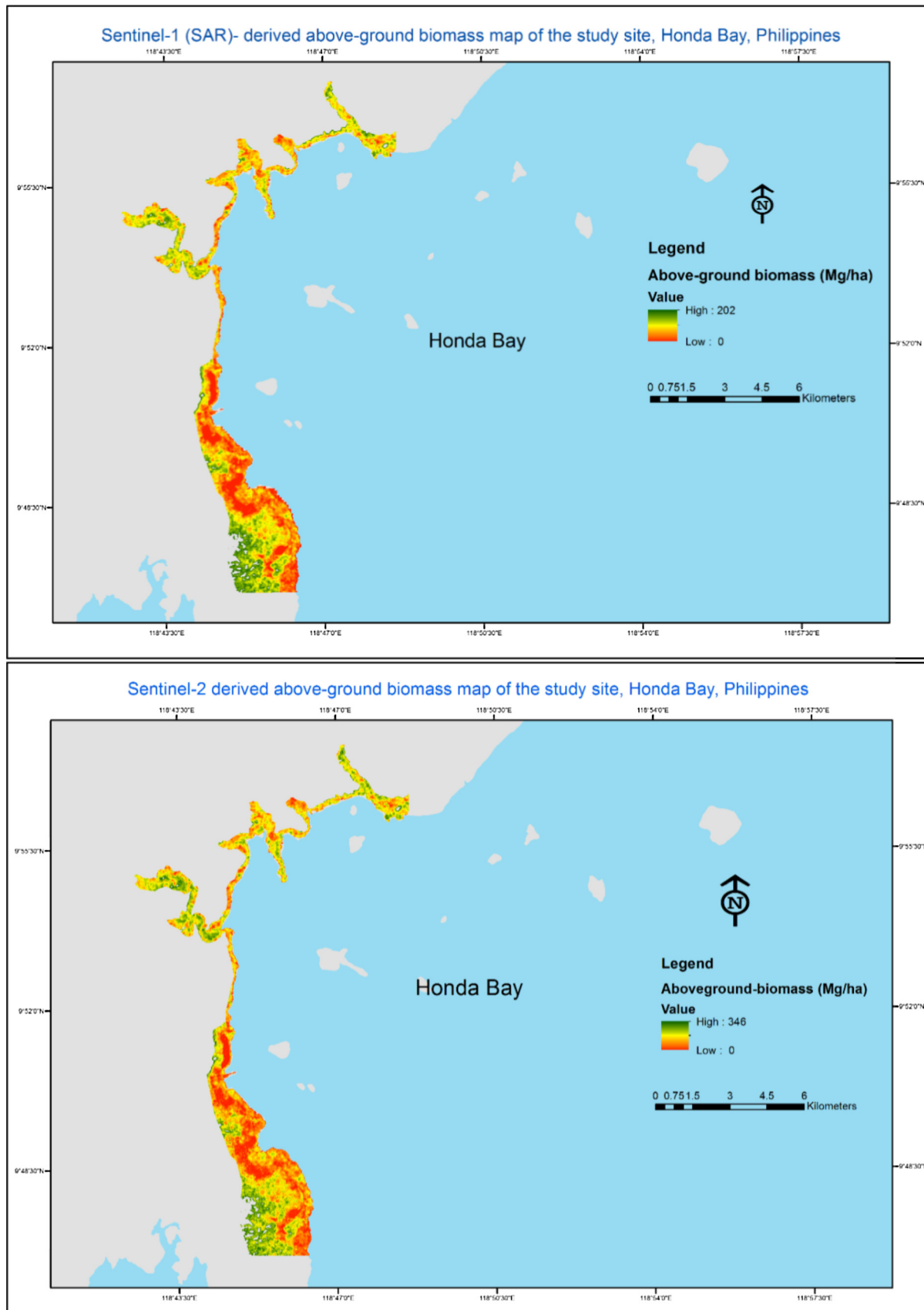


Fig. 8. Predicted maps of above-ground biomass in the study site derived from biomass models from a) Sentinel-1 SAR channels (top, equation 6) and b) Sentinel-2 multispectral bands (bottom, Eq. (7)).

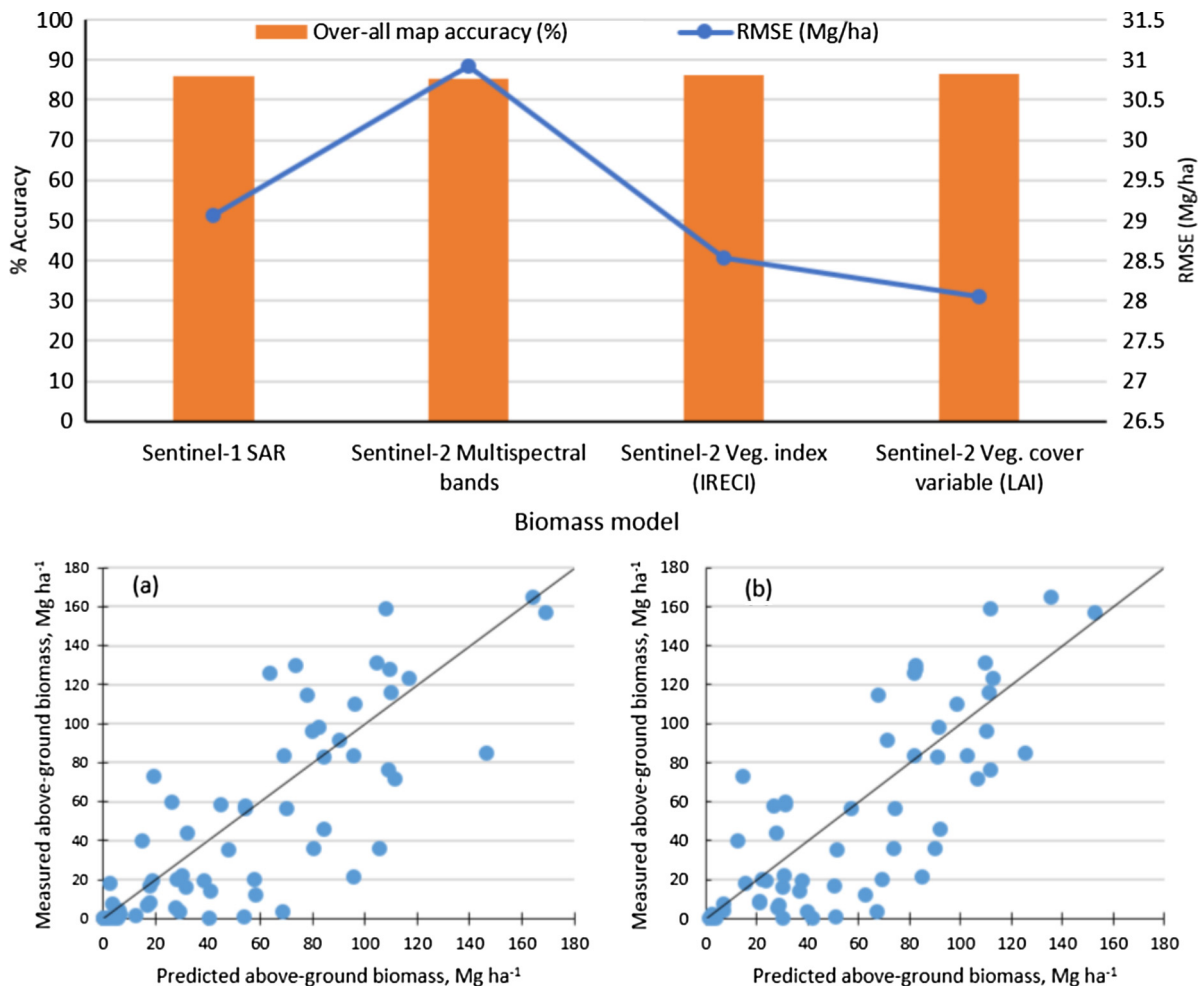


Fig. 9. Accuracy assessment of predicted biomass maps produced from the four Sentinel-based models (top panel). Scatter plots of observed and predicted biomass values correspond to (a) Sentinel-1-based map, (b) Sentinel-2 multispectral band-based map. Straight lines are 1:1 correspondence between observed and predicted biomass values.

(36.13–38.96 Mg ha⁻¹) but lowest in Sentinel LAI-derived biomass map. For coconut plantation biomass, Sentinel-2 optical bands-derived biomass map had the lowest prediction error (21.42 Mg ha⁻¹) while the vegetation index (IRECI)-derived biomass map had the highest error (26.7 Mg ha⁻¹). The SAR-derived biomass map had the lowest biomass prediction error for aquaculture pond, salt pond and cleared mangrove, that are all low biomass area, if not devoid of vegetation. Sentinel-2 band-derived biomass map had the highest prediction error for the retrieval of biomass from cleared mangrove (25.7 Mg ha⁻¹) compared to the three other biomass maps which had almost similar prediction error (3.5–4.5 Mg ha⁻¹).

4. Discussion

4.1. Relationship of field biomass with sentinel SAR polarisations and multispectral bands

Single-date SAR VH channel had a higher correlation with biomass than VV polarisation. However, the combination of multi-temporal VH and VV polarisations correlated better with biomass than single-date SAR imagery. Proisy et al. (2003) also reported similar observation for the C-band of the airborne-AIRSAR where cross-polarised HV channel had better correlation with biomass than co-polarised VV channel for both mangrove forests in Northern Australia and French Guiana. Also, Kumar et al. (2012) found

that multi-date Envisat ASAR images had a better correlation than single-date ASAR image in retrieving tropical forest biomass in India.

Bands in the Red edge (B6 and B7) and NIR (B8 and B8a) had a higher correlation with above-ground biomass than bands in the visible (B2, B3, B4) and short wave infrared (B11, B12) regions. Band combination in the Red edge (B5 and B6), as well as NIR (B8) and SWIR (B12) bands combination, had strong and better correlation with above-ground biomass than individual bands and other band combinations. The red edge and NIR regions are bands known to correlate well with biomass (Sibanda et al., 2015; Dube et al., 2016). In addition, among the Sentinel-derived vegetation indices, NDI45 and IRECI gave the highest correlation with biomass compared to NDVI and other vegetation index evaluated. NDI45 and IRECI are vegetation indices that use red edge bands which are known to relate well with biomass as mentioned above. Also, Leaf Area Index (LAI) had better correlation with biomass ($r = 0.80$) than the other vegetation cover biophysical variables evaluated. This is consistent with the findings of Dusseux et al. (2015) where correlation with biomass was highest with LAI than the other biophysical variable tested (i.e. fPAR). LAI gives information on the density of vegetation and describes more accurately the status of vegetation compared to other canopy variables (Dusseux et al., 2015).

Among the Sentinel predictor groups, the highest correlation with biomass was obtained when elevation was included as a

covariate. This is consistent with the results of [Jachowski et al. \(2013\)](#) for their mangrove biomass estimation in Thailand where the best biomass model was from the combination of multispectral bands and elevation, as well as with the results of [Dube and Mutanga \(2016\)](#) for their biomass and carbon stocks estimation of forest plantation species in South Africa. Elevation and tree height in mangrove area are related ([Simard et al., 2006; Fatoyinbo et al., 2008; Aslan et al., 2016](#)) probably due to mangrove's very close distance to the sea where elevation is usually set as zero. Tree height and biomass are allometrically related ([Cintron and Novelli, 1984; Chave et al., 2005; Komiya et al., 2005](#)).

4.2. Accuracy assessment of biomass prediction

The LAI-based model derived from the Sentinel-2 image was more accurate in predicting the overall above-ground biomass of the different coastal land uses studied, out-performing the models based on SAR raw polarisation backscatter, raw multispectral bands and multispectral-based vegetation index. The lowest accuracy was observed for the optical band-based model. Comparing the prediction per land use, the LAI-based model was also the best model for predicting mangrove biomass. The result is consistent with the study of [Dusseux et al. \(2015\)](#) and [Saatchi et al. \(2007\)](#) where LAI-based biomass model also gave the highest prediction for biomass compared to models based on vegetation index and other vegetation cover variables. However, the Sentinel SAR-based model was more accurate in predicting the biomass in the usually deficient to low vegetation cover non-forest replacement land uses such as abandoned aquaculture pond, cleared mangrove and abandoned salt pond. This is probably due to its ability to accurately detect non-vegetated areas such as water and open area whose surface are smooth to radar wave and with low backscatter coefficient compared to vegetation ([Kumar et al., 2012, 2015; Sinha et al., 2015](#)). C-band SAR, as in the case of Sentinel-1, is favoured for biomass study of low biomass sites such as forest clearings, grassland and forest regeneration sites because of its stronger backscattering in these areas compared to L and P bands ([Sinha et al., 2015](#)).

We found that using Sentinel-1 SAR and Sentinel-2 multispectral imagery data can give satisfactory results in the retrieval and predictive mapping of the above-ground biomass of mangroves and the replacement non-forest land uses, especially with the inclusion of elevation data. Agreement/correlation of predicted and observed biomass values from the Sentinel-1 SAR biomass model was 0.83. This value is almost similar to the value reported for Radarsat SAR (0.84) reported by [Li et al. \(2007\)](#) but lower than the value reported for PALSAR (0.91) by [Thapa et al. \(2015\)](#). Sentinel-1 and Radarsat are both in C-band, which has a shorter wavelength than the L-band in PALSAR that has higher canopy penetration capability ([Sinha et al., 2015](#)). For Sentinel-2 biomass models, the agreement between the predicted and observed values was 0.83. This value is the same for biomass prediction using ALOS VNIR-2 reported by [Wicaksono et al. \(2016\)](#) but slightly lower than the biomass model from SPOT (~0.85) given in [Pham and Brabyn \(2017\)](#); slightly higher than the biomass model derived from GeoEye-1 (0.81) reported by [Jachowski et al. \(2013\)](#), higher than Landsat-based model (0.67) reported by [Li et al. \(2007\)](#), but lower than the IKONOS-based model (0.93) reported by [Proisy et al. \(2007\)](#). Overall, the results we obtained are comparable to the previous studies above ([Table 6](#)).

However, one of the key benefits that come with using Sentinel imagery is that both the SAR and multispectral images are available, is free of charge, comes with open-source processing software (SNAP) and has a discussion forum for queries. This availability is important especially in developing countries in the tropics where

Table 6
Satellite-based biomass retrieval and mapping studies in mangrove area.

Sensor	Correlation/agreement of predicted and observed values	RMSE (Mg/ha)	Source
<i>Radar</i>			
Sentinel-1 SAR	0.83	27.75	<i>This study</i>
SRTM SAR	0.50	146.88	Aslan et al. (2016)
PALSAR	0.91	28.39	Thapa et al. (2015)
Radarsat SAR	0.84	9.46	Li et al. (2007)
SRTM SAR	0.82	20–40	Simard et al. (2006)
<i>Multispectral</i>			
Sentinel-2	0.83	28.02	<i>This study</i>
SPOT	~0.85	78.2	Pham and Brabyn (2017)
ALOS VNIR-2	0.83	Not reported	Wicaksono et al. (2016)
GeoEye	0.81	53.4	Jachowski et al. (2013)
IKONOS	0.93	42	Proisy et al. (2007)
Landsat	0.67	7.38	Li et al. (2007)

funds for the imagery and software procurement are limited and where there is persistent cloud cover, especially during rainy season. Also, compared to other free imagery, Sentinel-1 and Sentinel-2 have also higher spatial and temporal resolutions. Sentinel imagery have larger swath width compared to commercial imagery, which can be very useful in mapping for regional and national coverage. Potential issues with the use of Sentinel imagery may include difficulty in downloading and pre-processing of the imagery due to large imagery files (from the many bands and larger swath width), especially with the increased demand for the imagery in the future. These can be an issue for developing countries with slow internet connection and limited funding for the procurement of high-speed computer processor and larger memory.

It is acknowledged, however, that our estimations are not from destructive sampling and our benchmark/reference values are from field measurements. The true accuracy of models depends on how accurate our field-based measurements are. The agreement/correlation between our predicted and observed biomass values (i.e. 0.82 to 0.83) suggest that there is great potential for the retrieval and mapping of biomass in mangrove area in using the Sentinel imagery. The method we used in the study allowed us to generate cross-validated coastal biomass maps predicted from this free, open-source imagery. The predictive biomass maps we produced could be used as a baseline for which to compare results from future intervention such as reforestation.

Furthermore, Sentinel-1A was launched on April 3, 2014. The earliest available image that covered our study site was only on October 31, 2015. The three Sentinel-1A images used in the study were, in fact, the earliest first three images in GRD mode available for the study site. On the other hand, Sentinel-2A was launched on June 23, 2015. The earliest available Sentinel-2A image that covered the study site was only on January 12, 2016. The next earliest dates were February 11, 2016 and April 11, 2016. However, the images for January and February 2016 were both cloudy, thus the April 11, 2016 image was the one used for the study. Therefore, the imagery data used in the study were the closest to the field data acquisition time. We acknowledge the time elapsed between the field data collection and image acquisition (i.e. three to five months for Sentinel-1, and eight months for Sentinel-2). However, considering the available Sentinel images for the study site, it was assumed that the difference in field biomass is still negligible after three to eight months have passed (i.e. field data collection was conducted from June 2015 to July 2015). The mangrove forests and coconut plantation that we studied are all mature stands and presumably in a steady state. Also, five (i.e. December, January,

February, March and April) of the eight months elapsed time were dry season months where growth is minimum. Indeed, Proisy et al. (2007) in mapping the mangrove biomass in French Guiana also considered the time difference of 1 year between field data acquisition and imagery date as "not required" for biomass value adjustment. Future studies should consider using Sentinel images as close as possible to the field data collection to avoid the assumption that was made, considering that the Sentinel-1 and Sentinel-2 are now on their routine data collection.

5. Conclusion

Sentinel-1 (SAR) and Sentinel-2 (multispectral) image data can be used for biomass retrieval and mapping of the coastal land uses, mangrove and non-mangrove alike, of Honda Bay and adjacent coastal areas in Puerto Princesa City, Philippines. The prediction accuracy is comparable to imagery from current commercial sensors. High correlation values ($r = 0.84$) between biomass and Sentinel imagery data were obtained from the combination of dual-date SAR VH and VV channels, red and red edge bands, red edge-based vegetation indices and leaf area index, respectively. The developed Sentinel-based models have prediction errors of $<29 \text{ Mg ha}^{-1}$ while the output predictive biomass maps had prediction accuracy of 85.3–86.6% and agreement/correlation (r) of observed and predicted biomass value of 0.82–0.84. The Sentinel SAR-based model was more accurate in predicting the biomass in the usually deficient to low vegetation cover non-forest replacement land uses such as abandoned aquaculture pond, cleared mangrove and abandoned salt pond. The study indicates satisfactory results and suggests good potential for mapping the coastal land uses in the study area. The free and open-source Sentinel imagery in both SAR and multispectral data and the associated open-source SNAP software should encourage the conduct of biomass mapping and monitoring in the coastal zone of resource-poor countries, especially in the tropics. In addition, the methods developed might be used to map and estimate the above-ground biomass of mangrove and non-forest land uses in the coastal zone similar to the study site. Follow-up studies should aim for the generation of DEM from Sentinel-1 InSAR in order to test its capability for biomass retrieval and mapping in combination with Sentinel backscatter and multispectral data. In addition, the accuracy of the map might be improved with additional plots distributed strategically in areas far from the current plots, and additional sites for each land use especially for coconut plantation, abandoned salt pond and cleared mangrove. Lastly, the use of various data transformation techniques, as well as non-linear multiple regression forms, should also be pursued with the aim of finding the highest correlation for predicted and observed value, and lower prediction error compared to the current values.

Acknowledgement

We would like to thank Australia Awards Scholarship for the full-time scholarship of the first author (ST000FN15) and for funding his round-trip airfares during the fieldwork in the Philippines, and the University of Southern Queensland, Australia for contributing some funds for the study. We are also grateful to Ecosystems Research and Development Bureau (ERDB) management and staff in the Philippines for providing logistics and fieldwork support. The help and company of Elmer Caliwagan, Leoncio "Piolo" Baguhin, Digno Garcia, Perfecto Melo, Artemio Ortega and Donald Apan during the fieldwork are highly appreciated. We also thank the village officials and residents of San Jose, Tagburos, Santa Lourdes, Bacungan, Santa Cruz and Salvacion, for providing us access and assistance in the field and for giving us information on land use

history of the area. We also thank ESA for providing us access to their Sentinel-1 and Sentinel-2 imagery and the SNAP software, as well as NASA for the SRTM 1 arc-second DEM. We also like to thank Dr. Rudolf Espada of USQ for critically editing the English language of the manuscript. Finally, our thanks to the two anonymous reviewers for their critical but helpful comments and suggestions, which greatly helped in improving the manuscript.

References

- Abino, A.C., Castillo, J.A.A., Lee, Y.J., 2014. Species diversity, biomass, and carbon stock assessments of a natural mangrove forest in palawan, philippines. *Pak. J. Bot.* 46 (6), 1955–1962.
- Alongi, D., 2009. The Energetics of Mangrove Forests. Springer, Netherlands.
- Aslan, A., Rahman, A.F., Warren, M.W., Robeson, S.M., 2016. Mapping spatial distribution and biomass of coastal wetland vegetation in Indonesian Papua by combining active and passive remotely sensed data. *Remote Sens. Environ.* 183, 65–81.
- Bhomia, R.K., MacKenzie, R.A., Murdiyarso, D., Sasmito, S.D., Purbopuspito, J., 2016. Impacts of land use on Indian mangrove forest carbon stocks: implications for conservation and management. *Ecol. Appl.* 26 (5), 1396–1408.
- Brown, S., 1997. Estimating Biomass and Biomass Change of Tropical Forests: A Primer. vol. 134, Food & Agriculture Org.
- Chave, J., Andalo, C., Brown, S., Cairns, M.A., Chambers, J.Q., Eamus, D., Fölster, H., Fromard, F., Higuchi, N., Kira, T., Lescure, J.-P., Nelson, B.W., Ogawa, H., Puig, H., Riéra, B., Yamakura, T., 2005. Tree allometry and improved estimation of carbon stocks and balance in tropical forests. *Oecologia* 145 (1), 87–99.
- Christensen, L.K., Bennedsen, B.S., Jørgensen, R.N., Nielsen, H., 2004. Modelling nitrogen and phosphorus content at early growth stages in spring barley using hyperspectral line scanning. *Biosyst. Eng.* 88 (1), 19–24.
- Cintron, G., Novelli, Y.S., 1984. 'Methods for Studying Mangrove Structure', in *Mangrove Ecosystem: Research Methods*, Unesco, pp. 91–113.
- Clough, B.F., Scott, K., 1989. Allometric relationships for estimating above-ground biomass in six mangrove species. *For. Ecol. Manage.* 27 (2), 117–127.
- Donato, D.C., Kauffman, J.B., Murdiyarso, D., Kurnianto, S., Stidham, M., Kanninen, M., 2011. Mangroves among the most carbon-rich forests in the tropics. *Nat. Geosci.* 4 (5), 293–297.
- Dube, T., Mutanga, O., 2015. 'Investigating the robustness of the new Landsat-8 Operational Land Imager derived texture metrics in estimating plantation forest aboveground biomass in resource constrained areas', *ISPRS. J. Photogrammetry Remote Sens.*, vol. 108, no. Supplement C, pp. 12–32.
- Dube, T., Mutanga, O., 2016. 'The impact of integrating WorldView-2 sensor and environmental variables in estimating plantation forest species aboveground biomass and carbon stocks in uMgeni Catchment, South Africa', *ISPRS J. Photogrammetry Remote Sens.*, vol. 119, no. Supplement C, pp. 415–25.
- Dube, T., Gara, T.W., Mutanga, O., Sibanda, M., Shoko, C., Murwira, A., Masocha, M., Ndaimani, H., Hatendi, C.M., 2016. 'Estimating forest standing biomass in savanna woodlands as an indicator of forest productivity using the new generation WorldView-2 sensor', *Geocarto International*, pp. 1–11.
- Duncan, C., Primavera, J.H., Pettorelli, N., Thompson, J.R., Loma, R.J.A., Koldewey, H.J., 2016. Rehabilitating mangrove ecosystem services: a case study on the relative benefits of abandoned pond reversion from Panay Island, Philippines. *Mar. Pollut. Bull.* 109 (2), 772–782.
- Dusseux, P., Hubert-Moy, L., Corpetti, T., Vertès, F., 2015. Evaluation of SPOT imagery for the estimation of grassland biomass. *Int. J. Appl. Earth Obs. Geoinf.* 38, 72–77.
- ESA, 2016. Sentinels Scientific Data Hub, European Space Agency, viewed August 1, 2016, <<https://scihub.copernicus.eu/>>.
- FAO, 2007. The World's Mangroves 1980–2005. Food and Agriculture Organisation, Rome, Italy.
- Fatoyinbo, T.E., Simard, M., Washington-Allen, R.A., Shugart, H.H., 2008. Landscape-scale extent, height, biomass, and carbon estimation of Mozambique's mangrove forests with Landsat ETM+ and Shuttle Radar Topography Mission elevation data. *J. Geophys. Res.: Biogeosci.* 113 (G2), G02S6.
- Hall, M., Frank, E., Holmes, G., Pfahringer, B., Reutemann, P., Witten, I.H., 2009. The WEKA data mining software: an update. *ACM SIGKDD Explorations Newslett.* 11 (1), 10–18.
- Howard, J., Hoyt, S., Isensee, K., Telszewski, M., Pidgeon, E., 2014. Coastal blue carbon: methods for assessing carbon stocks and emissions factors in mangroves, tidal salt marshes, and seagrasses. *Conservation International, Intergovernmental Oceanographic Commission of UNESCO, International Union for Conservation of Nature*, Arlington, VA, USA.
- Jachowski, N.R.A., Quak, M.S.Y., Friess, D.A., Duangnamon, D., Webb, E.L., Ziegler, A.D., 2013. Mangrove biomass estimation in Southwest Thailand using machine learning. *Appl. Geogr.* 45, 311–321.
- Jacquemoud, S., Verhoef, W., Baret, F., Bacour, C., Zarco-Tejada, P.J., Asner, G.P., Francoise, C., Ustin, S.L., 2009. PROSPECT + SAIL models: a review of use for vegetation characterization (Supplement 1). *Remote Sens. Environ.* 113, S56–S66.
- Kauffman, J.B., Donato, D., 2012. Protocols for the measurement, monitoring and reporting of structure, biomass and carbon stocks in mangrove forests, Center for International Forestry Research (CIFOR), Bogor, Indonesia.

- Kauffman, J.B., Heider, C., Norfolk, J., Payton, F., 2013. Carbon stocks of intact mangroves and carbon emissions arising from their conversion in the Dominican Republic. *Ecol. Appl.* 24 (3), 518–527.
- Kauffman, J.B., Hernandez Trejo, H., del Carmen Jesus Garcia, M., Heider, C., Contreras, W.M., 2016. Carbon stocks of mangroves and losses arising from their conversion to cattle pastures in the Pantanos de Centla, Mexico. *Wetlands Ecol. Manage.* 24 (2), 203–216.
- Komiyama, A., Poungparn, S., Kato, S., 2005. Common allometric equations for estimating the tree weight of mangroves. *J. Trop. Ecol.* 21 (04), 471–477.
- Kovacs, J.M., Lu, X.X., Flores-Verdugo, F., Zhang, C., Flores de Santiago, F., Jiao, X., 2013. Applications of ALOS PALSAR for monitoring biophysical parameters of a degraded black mangrove (*Avicennia germinans*) forest. *ISPRS J. Photogrammetry Remote Sens.*, 82, Supplement C, 102–11.
- Kumar, L., Sinha, P., Taylor, S., Alqurashi, A.F., 2015. Review of the use of remote sensing for biomass estimation to support renewable energy generation. *J. Appl. Remote Sens.*, 9(1) 097696.
- Kumar, S., Pandey, U., Kushwaha, S.P., Chatterjee, R.S., Bijkar, W., 2012. Aboveground biomass estimation of tropical forest from Envisat advanced synthetic aperture radar data using modeling approach. *J. Appl. Remote Sens.* 6 (1), 063588.
- Li, X., Gar-On Yeh, A., Wang, S., Liu, K., Liu, X., Qian, J., Chen, X., 2007. Regression and analytical models for estimating mangrove wetland biomass in South China using Radarsat images. *Int. J. Remote Sens.* 28 (24), 5567–5582.
- Liu, C., 2016. Analysis of Sentinel-1 SAR Data for Mapping Standing Water in the Twente Region Masters Thesis. University of Twente, Enschede, The Netherlands.
- Lu, D., Mausel, P., Brondizio, E., Moran, E., 2004. Relationships between forest stand parameters and Landsat TM spectral responses in the Brazilian Amazon Basin. *For. Ecol. Manage.* 198 (1–3), 149–167.
- Maraseni, T.N., Cockfield, G., Apan, A., 2005. Community based forest management systems in developing countries and eligibility for clean development mechanism. *J. Forest Livelihood* 4 (2), 31–42.
- Maraseni, T.N., Mathers, N.J., Harms, B., Cockfield, G., Apan, A., Maroulis, J., 2008. Comparing and predicting soil carbon quantities under different land-use systems on the Red Ferrosol soils of southeast Queensland. *J. Soil Water Conserv.* 63 (4), 250–256.
- Ong, J.E., Gong, W.K., Wong, C.H., 2004. Allometry and partitioning of the mangrove, *Rhizophora apiculata*. *For. Ecol. Manage.* 188 (1–3), 395–408.
- PAGASA, 2016. Climatological Normals, Philippine Atmospheric, Geophysical and Astronomical Services Administration. <<http://web.pagasa.dost.gov.ph/index.php/climate/climatological-normals>> (accessed 31 March, 2016).
- Pham, L.T.H., Brabyn, L., 2017. Monitoring mangrove biomass change in Vietnam using SPOT images and an object-based approach combined with machine learning algorithms. *ISPRS J. Photogrammetry Remote Sens.* 128(Supplement C) 86–97.
- Phang, V.X.H., Chou, L.M., Friess, D.A., 2015. Ecosystem carbon stocks across a tropical intertidal habitat mosaic of mangrove forest, seagrass meadow, mudflat and sandbar. *Earth Surf. Proc. Land.* 40 (10), 1387–1400.
- Proisy, C., Couteron, P., Fromard, F., 2007. Predicting and mapping mangrove biomass from canopy grain analysis using Fourier-based textural ordination of IKONOS images. *Remote Sens. Environ.* 109 (3), 379–392.
- Proisy, C., Mitchell, A., Lucas, R., Fromard, F., Mougin, E., 2003. Estimation of Mangrove Biomass using Multifrequency Radar Data: Application to Mangroves of French Guiana and Northern Australia, Mangrove 2003 Conference, Bahia, Brazil.
- Richards, D.R., Friess, D.A., 2016. Rates and drivers of mangrove deforestation in Southeast Asia, 2000–2012. *Proc. Natl. Acad. Sci.* 113 (2), 344–349.
- Saatchi, S.S., Houghton, R.A., Dos Santos Alvalá, R.C., Soares, J.V., Yu, Y., 2007. Distribution of aboveground live biomass in the Amazon basin. *Glob. Change Biol.* 13 (4), 816–837.
- Samalca, I.K., 2007. Estimation of Forest Biomass and its Error: A Case in Kalimantan, Indonesia, Unpublished MSc. Thesis, ITC the Netherlands, Enschede.
- Sarker, M.L.R., Nichol, J., Ahmad, B., Busu, I., Rahman, A.A., 2012. Potential of texture measurements of two-date dual polarization PALSAR data for the improvement of forest biomass estimation. *ISPRS J. Photogrammetry Remote Sens.* 69 (Supplement C) 146–66.
- Sentinel-1_Team, 2015. Sentinel-1 User Handbook, European Space Agency.
- Sentinel-2_Team, 2015. Sentinel-2 User Handbook, European Space Agency.
- Sibanda, M., Mutanga, O., Rouget, M., 2015. Examining the potential of Sentinel-2 MSI spectral resolution in quantifying above ground biomass across different fertilizer treatments. *ISPRS J. Photogrammetry Remote Sens.* 110, 55–65.
- Simard, M., Zhang, K., Rivera-Monroy, V.H., Ross, M.S., Ruiz, P.L., Castañeda-Moya, E., Twilley, R.R., Rodriguez, E., 2006. Mapping height and biomass of mangrove forests in everglades national park with SRTM elevation data. *Photogrammetric Eng. Remote Sens.* 72 (3), 299–311.
- Sinha, S., Jegannathan, C., Sharma, L.K., Nathawat, M.S., 2015. A review of radar remote sensing for biomass estimation. *Int. J. Environ. Sci. Technol.* 12 (5), 1779–1792.
- SNAP, 2016. Sentinels Application Platform software ver. 4.0.0, European Space Agency.
- Stringer, C.E., Trettin, C.C., Zarnoch, S.J., Tang, W., 2015. Carbon stocks of mangroves within the Zambezi River Delta, Mozambique. *Forest Ecol. Manage.* 354, 139–148.
- Thapa, R.B., Watanabe, M., Motohka, T., Shimada, M., 2015. Potential of high-resolution ALOS-PALSAR mosaic texture for aboveground forest carbon tracking in tropical region. *Remote Sens. Environ.* 160, 122–133.
- Tue, N.T., Dung, L.V., Nhuan, M.T., Omori, K., 2014. Carbon storage of a tropical mangrove forest in Mui Ca Mau National Park, Vietnam. *CATENA* 121, 119–126.
- USGS, 2016. EarthExplorer, United States Geological Service, viewed August 1, 2016, <<https://earthexplorer.usgs.gov/>>.
- Veci, L., 2015. Sentinel-1 Toolbox: SAR Basics Tutorial, ARRAY Systems Computing, Inc. and European Space Agency.
- Vien, N., Sasmito, S.D., Murdiyarto, D., Purbopuspito, J., MacKenzie, R.A., 2016. Carbon stocks in artificially and naturally regenerated mangrove ecosystems in the Mekong Delta. *Wetlands Ecol. Manage.* 24 (2), 231–244.
- Wicaksono, P., Danoedoro, P., Hartono, Nehren, U., 2016. Mangrove biomass carbon stock mapping of the Karimunjawa Islands using multispectral remote sensing. *Int. J. Remote Sens.* 37 (1), 26–52.